A Weather Radar Simulator for the Evaluation of Polarimetric Phased Array Performance

Andrew D. Byrd, *Student Member, IEEE*, Igor R. Ivić, Robert D. Palmer, *Senior Member, IEEE*, Bradley M. Isom, *Member, IEEE*, Boon Leng Cheong, Alexander D. Schenkman, and Ming Xue

***Abstract*—A radar simulator capable of generating time series data for a polarimetric phased array weather radar has been designed and implemented. The received signals are composed from a high-resolution numerical prediction weather model. Thousands of scattering centers (SCs), each with an independent randomly generated Doppler spectrum, populate the field of view of the radar. The moments of the SC spectra are derived from the numerical weather model, and the SC positions are updated based on the 3-D wind field. In order to accurately emulate the effects of the system-induced cross-polar contamination, the array is modeled using a complete set of dual-polarization radiation patterns. The simulator offers reconfigurable element patterns and positions and access to independent time series data for each element, resulting in easy implementation of any beamforming method. It also allows for arbitrary waveform designs and is able to model the effects of quantization on waveform performance. Simultaneous, alternating, quasi-simultaneous, and pulse-to-pulse phase-coded modes of polarimetric signal transmission have been implemented. This framework allows for realistic emulation of the effects of cross-polar fields on weather observations, as well as the evaluation of possible techniques for the mitigation of those effects.**

***Index Terms*—Radar, meteorological radar, polarimetry, radar polarimetry, phased arrays, simulation, computer simulation.**

I. Introduction

METEOROLOGICAL radars are powerful instruments for the remote sensing of the atmosphere because they are capable of weather surveillance which covers vast areas. At the same time, the accuracy of measurements produced by these instruments is heavily dependent on the properties of the instrument itself (e.g., operating frequency and radiation fields), as well as accurate calibration and continuous maintenance. Moreover, the relationship between radar measurables and physical characteristics of precipitation (e.g., rainfall rate) depends on the assumed model of observed phenomena and therefore is not unique. For these reasons, weather radar simulators are useful because they provide complete control of a synthetic weather environment and properties of radar used to survey this environment. Such a level of control allows for separation and evaluation of the effects of sensor characteristics (e.g., operating frequency and radiation patterns) on the radar measurables and variation of the microphysical parameters of precipitation (physical state, size, shape, and number density of the hydrometeors).

Weather radar simulators may be classified by whether they produce time series data or directly simulate products such as Doppler moments and polarimetric variables. The latter type of simulator has been used for a number of applications such as rain rate measurement (see [1]–[4]), sensitivity studies [5], tornadic signature detection [6], feasibility studies for airborne radars [7], and polarimetric data assimilation [8]. They are useful for any application where the only requirement for the desired study is a plausible field of radar observables (often reflectivity only) given some specified set of conditions. They are generally less computationally intensive than those that produce time series data. Unfortunately, several of the techniques that are of principal interest to studies of polarimetric bias mitigation, such as phase-coded simultaneous horizontal and vertical (PCSHV) (see [9]–[11]) and quasi-simultaneous horizontal and vertical (QSHV) (see [10] and [12]) transmit modes, require signal modeling at the time series level.

Time series simulators are typically based on the concept of the "scattering center" (SC), which originated with researchers working with wind profilers. SC-based simulators populate the simulation space with artificial scatterers representing some ensemble average of the radar profile of the hydrometeors (or, in the case of wind profilers, refractivity gradients) in the surrounding region of space. Holdsworth and Reid [13] and, more recently, Venkatesh and Frasier [14] implemented this concept from a Lagrangian field specification perspective in which the SCs moved through the simulation space with the wind field. Later, Muschinski *et al.* [15] implemented a similar principle from a Eulerian field specification perspective in which their SCs remained fixed in space over the course of the simulation. Time series simulators may be classified based on their fundamental SC mechanics. They can be sorted into two groups based on what each simulated SC represents. In the first category of simulator, which uses a homogenous scattering center (HSC) method, each SC represents a group of hydrometeors with single uniform diameter, shape, and orientation. The

Manuscript received November 15, 2015; revised January 29, 2016; accepted March 1, 2016. Date of publication April 6, 2016; date of current version May 24, 2016. This work was supported by the NOAA National Severe Storms Laboratory under Cooperative Agreement NA11OAR4320072.

A. D. Byrd is with the Advanced Radar Research Center and the School of Electrical and Computer Engineering, University of Oklahoma, Norman, OK 73019 USA (e-mail: adbyrd@ou.edu).

I. R. Ivić is with the Cooperative Institute for Mesoscale Meteorological Studies, University of Oklahoma, and also with the National Severe Storms Laboratory, National Oceanic and Atmospheric Administration, Norman, OK 73072 USA (e-mail: igor.ivic@noaa.gov).

R. D. Palmer is with the Advanced Radar Research Center and the School of Meteorology, University of Oklahoma, Norman, OK 73019 USA.

B. M. Isom is with the Atmospheric Measurement and Data Sciences, Pacific Northwest National Laboratory, Richland, WA 99352 USA.

B. L. Cheong is with the Advanced Radar Research Center, University of Oklahoma, Norman, OK 73019 USA.

A. D. Schenkman is with the Center for Analysis and Prediction of Storms, University of Oklahoma, Norman, OK 73072 USA.

M. Xue is with the Center for Analysis and Prediction of Storms, University of Oklahoma, Norman, OK 73072 USA, and also with University of Oklahoma School of Meteor, Adv. Radar Research Center, Norman, OK 73019 USA.

Color versions of one or more of the figures in this paper are available online at http://ieeexplore.ieee.org.

Digital Object Identifier 10.1109/TGRS.2016.2538179

second type uses a bulk scattering center (BSC) method. In this method, each SC represents a group of hydrometeors that follow some specified heterogeneous distribution of diameters, shapes, and orientations. HSC-based simulators excel as a tool for studying the effects of physical attributes of precipitation on radar signatures, due to the fact that they allow for fine control of the drop size distribution (DSD), as well as the simulation of precipitation with mixed physical states. However, the emulation of enough SCs to adequately represent the desired distribution of physical characteristics creates heavy computational demands. For this reason, many of them (see [16]–[18]) only emulate single-resolution volumes. While larger scale simulations based on an HSC method have been developed [19], computational resources are still a concern for this type of simulation. In particular, if a simulator is to focus primarily on high-fidelity studies of radar system effects, which will require the dedication of a significant amount of computing power, there are clear advantages to making some sacrifices in weather simulation fidelity in order to gain computational efficiency. This can be achieved through BSC-based simulations.

One key difference between HSC- and BSC-based simulators is how randomness is introduced at the microphysical level. In HSC systems, this occurs through the population of HSCs with random microphysical properties sampled from a distribution based on the weather model. In BSC systems, because each SC has some deterministically calculated set of expected radar observables (generally based on integration of scattering parameters over a DSD calculated from a weather model), randomness is introduced (if at all) by combining the calculated observables with a weather-like random signal model. The seminal work of Zrnic [20] on the simulation of weather-like signals outlines the basic process of generating single-polarization radar time series as colored Gaussian noise given the preset true values of Doppler moments. In a later paper, Chandrasekhar and Bringi [16] generated the time series through integration of DSD functions and Zrnic's method, taking the first steps toward coupling the statistical time series generation method with physical models of weather. Galati and Pavan [21] provided an extension of Zrnic's signal generation method to polarimetric radars in their paper discussing methods for efficient generation of these signals and the mathematical methods to produce horizontal/vertical (H/V) signal pairs with a specified scaling, phase delay, and correlation coefficient.

A dissertation by Torres [22] is the first example of an SC-based simulator that uses a weather-like signal model to emulate random microphysical properties of the weather as opposed to using the model to directly represent the signal received by the radar. The system parameters of the radar such as transmitted waveform specifications were then used to take a weighted average of the SC amplitudes and phases, produced using the Zrnic and Galati and Pavan methods. Cheong *et al.* (see [23] and [24]), on the other hand, made use of the Lagrangian SC framework developed by Holdsworth and Reid by randomly populating the simulation space with BSCs that moved according to the simulated wind field specified by the Advanced Regional Prediction System (ARPS) weather prediction model (see [25] and [26]). Rather than implementing Doppler velocities through the parameters of weather-like signals coupled to the SCs, Cheong *et al.* did not simulate any microphysical randomness, modeling the SCs as having a deterministic position-dependent amplitude and phase and allowing the Doppler velocities to emerge through the motion of the SCs. This was also the first of the time series simulators to derive its signals from a numerical weather prediction (NWP) model. While this had already been common in simulators that produce Doppler moments and polarimetric variables directly, time series simulators had generally been used for signal processing studies (e.g., evaluation of radar observable estimation errors) in which it was not necessary to realistically simulate a large region of the atmosphere. The BSC framework (with weather-like signal-based microphysical randomness) was later combined with NWP-based atmospheric simulations and used to simulate polarimetric radar returns in studies by May [27] and Lischi *et al.* [28].

Recent introduction of polarimetric phased array radar (PPAR) technology for weather observations (see [29] and [30]) demands new considerations for accurate weather radar system simulation. One of the most prominent issues with PPAR is the fact that a portion of the energy transmitted into the H-polarized antenna port is radiated as cross-polar V field, and vice versa. Likewise, on receive, a portion of the H-polarized radiation incident on the array is received by the V port, and vice versa. For a well-designed reflector antenna, this effect can be neglected [31], but it cannot be neglected for PPAR antennas (see [32]–[35]). Thus, in PPAR systems, the cross-polar contamination results in significant biases (referred to as the cross-coupling biases) in the estimates of polarimetric variables. There has been significant work to characterize these biases using theoretical analysis (see [32]–[35]), but notably less using simulations (see [11], [12], and [36]). None of these studies, however, evaluates the cross-coupling biases from the simulated fields of weather-like radar observables. The problem of cross-coupling biases becomes even more important given that the efforts toward future upgrade of the national weather radar network Weather Surveillance Radar—1988 Doppler (WSR-88D) have focused on the concept of a multifunction phased array radar (MPAR) (see [29] and [30]). Hence, one of the key aspects to maintaining or improving upon the quality of meteorological data provided by the WSR-88D is the ability to make accurate polarimetric measurements using MPAR. Due to these problems, the 2nd MPAR Symposium [37] identified the polarimetric capability to be the most challenging technical issue for future MPAR. Consequently, it becomes important to evaluate the performance of PPAR on the simulated fields of weather-like radar observables. Of the simulators surveyed herein, only two claim to be able to emulate phased arrays. The simulator implemented by Li *et al.* [19] was designed to simulate airborne polarimetric array radars, but the main subjects of interest in the authors' investigations were the impacts of the airborne platform and various microphysical effects, on the polarimetric signals. Therefore, they were able to simply use an illustrative array factor as the antenna pattern and assumed no presence of system-induced cross-polar fields. The simulator implemented by Cheong *et al.* [24] simulates arrays with greater flexibility, but still with significant limitations. This simulator operates through specification of the element positions rather than an array factor, and it is capable of generating a time series signal for each individual element. However, it also assumes no presence of cross-polar fields and only models imaging radars (it does not allow for beamforming on transmit). In addition, it only offers an incomplete polarimetric characterization of scatterers, implementing differential reflectivity, but not differential phase or correlation coefficient. The reasons presented earlier are the motivation for the development of weather radar simulator capable of modeling polarimetric phased arrays accurately enough to conduct a detailed study of their limitations or the proposed techniques to overcome them.

II. Atmospheric Simulation

A. Parameterization of Radar Observables

The simulator uses the output of the ARPS model (see [25] and [26]) to emulate realistic atmospheric conditions. However, this model does not directly provide the radar observables necessary to compose time series data. Rather, it provides meteorological information about the state of the atmosphere. This must be coupled with assumptions about the DSD, drop shape, and scattering regime of the precipitation present in the simulation volume in order to obtain the parameters necessary to compose a simulated radar return.

ARPS has seen prior use in weather radar simulations by May *et al.* [6], Cheong *et al.* [24], and Li *et al.* [19]. It is a fully compressible nonhydrostatic prediction model. It provides information on the physical state of the atmosphere in the form of a 3-D grid, including the components of the wind field u, v, and w; potential temperature θ; pressure p; mixing ratios for water vapor q_{V}, cloud water q_c, rainwater q_r, cloud ice q_i, snow q_s, and hail q_{H}; and turbulent kinetic energy (TKE) used by the 1.5-order subgrid-scale turbulent closure scheme (see [25], [26], and [38]). Currently, the simulator only makes use of the Kessler-type warm rain microphysics. The particular ARPS data set used to generate the simulations presented in this paper has a 25-m horizontal grid spacing and a stretched vertical grid spacing with a minimum of 20-m spacing at the surface. It is a simulation of a tornadic supercell thunderstorm initiated by a thermal bubble in a horizontally homogenous environment based on a sounding taken on May 20, 1977 in Del City, Oklahoma [39]. Additional information on the simulation can be found in Cheong *et al.* [24]. The simulations carried out to produce the examples presented later in this paper use a small swath of this volume of ARPS data containing the tornado producing hook echo.

The foundation for the conversion of the ARPS state variables into polarimetric radar observables is laid out by Jung *et al.* [40] as an intermediate step in a study of polarimetric radar data assimilation. Her work assumes a constrained version of the gamma DSD as proposed by Ulbrich [41], which is expressible as

$$N(D) = N_0 D^{\mu} \exp(-\Lambda D) \quad (0 < D < D_{\max}) \tag{1}$$

where D is the drop diameter; and N_0, Λ, and μ are the DSD parameters. N_0 (assuming only liquid precipitation) is assumed to have a fixed value of 8×10^6 m^{-4}. Λ varies based on q_r according to the following expression [42]:

$$\Lambda = \left(\frac{\pi \rho_r N_0}{\rho q_r}\right)^{0.25} \tag{2}$$

where ρ is the air density calculated based on p, θ, and the ideal gas law; and $\rho_r \approx 1000$ kg $\cdot$ m^{-3} is the density of liquid water. μ is estimated from Λ based on the following expression derived by Zhang *et al.* [43] through polynomial fitting on the results of disdrometer observation:

$$\mu = -0.016\Lambda^2 + 1.213\Lambda - 1.957. \tag{3}$$

In addition, Jung uses the following relation between drop diameter and axial ratio r derived by Zhang *et al.* [43]:

$$r = 1.0148 - 2.0465 \times 10^{-2} D - 2.0048 \times 10^{-2} D^2 + 3.095 \times 10^{-3} D^3 - 1.453 \times 10^{-4} D^4. \tag{4}$$

This relation is derived by solving the equilibrium expression for raindrop shape presented by Green [44] and performing a polynomial fit. This set of assumptions regarding DSD and drop shape, coupled with the T-matrix scattering model (see [45, Appendix 3]), yields the following results for horizontal reflectivity Z_{H} and vertical reflectivity Z_{V} after integration of the scattering parameters over the DSD:

$$Z_{\mathrm{H}} = \frac{4\lambda^4 \alpha_a^2 N_0}{\pi^4 |K_w|^2} \Lambda^{-(2\beta_a+1)} \Gamma(2\beta_a + 1) \text{ mm}^6\text{m}^{-3} \tag{5}$$

$$Z_{\mathrm{V}} = \frac{4\lambda^4 \alpha_b^2 N_0}{\pi^4 |K_w|^2} \Lambda^{-(2\beta_b+1)} \Gamma(2\beta_b + 1) \text{ mm}^6\text{m}^{-3} \tag{6}$$

where λ is the radar wavelength, $\alpha_a = \alpha_b = 4.28 \times 10^{-4}$, $\beta_a = 3.04$, and $\beta_b = 2.77$. Through the same process of integration, the specific differential phase K_{DP} can be expressed as

$$K_{\mathrm{DP}} = \frac{180\lambda}{\pi} N_0 \alpha_k \Lambda^{-(\beta_k+1)} \ {}^\circ\text{km}^{-1} \tag{7}$$

where $\alpha_k = 1.30 \times 10^{-5}$, and $\beta_k = 4.63$. Because the simulator does not model propagation effects directly, it is necessary to convert K_{DP} to differential phase Φ_{DP}. In order to achieve this, the K_{DP} values for the points in the rectangular ARPS grid are linearly interpolated to a spherical grid with the origin located at the center of the simulated radar's array face. These values are then numerically integrated along each radial from the origin to the furthest extent of the simulation volume. The resulting values of Φ_{DP} are then interpolated back to the rectangular ARPS grid for use in the simulation.

Jung does not provide a method for determining values of copolar correlation coefficient $|\rho_{\mathrm{HV}}(0)|$ from ARPS data. In order to calculate this parameter, the same assumptions about DSD and axial ratio were used as when calculating the other polarimetric parameters. However, the Rayleigh–Gans model rather than the T-matrix was used to calculate the scattering parameters for each drop size, as outlined by May [27, eqs. 2.23–2.29]. Rather than attempting to provide an analytical expression for $|\rho_{\mathrm{HV}}(0)|$, a numerical approach was taken. First, a family of DSDs was calculated over the full range of Λ values present in the ARPS model. For each of these DSDs, the following integral expression [45] was numerically solved:

$$|\rho_{\mathrm{HV}}(0)| = \frac{\left|\int_0^{D_{\mathrm{MAX}}} s_{\mathrm{HH}}^f(D) s_{\mathrm{VV}}^{f*}(D) N(D) dD\right|}{\sqrt{\int_0^{D_{\mathrm{MAX}}} \left|s_{\mathrm{HH}}^f\right|^2 N(D) dD \int_0^{D_{\mathrm{MAX}}} \left|s_{\mathrm{VV}}^f\right|^2 N(D) dD}} \tag{8}$$

where $s^f_{\mathrm{HH}}(D)$ and $s^f_{\mathrm{VV}}(D)$ are the horizontally and vertically copolar forward scattering parameters for a raindrop of diameter D. At each point in the ARPS grid, a ρ_{HV} value was then linearly interpolated from the precalculated integrals based on the value of Λ at that point.

One additional parameter that must be calculated from the ARPS table is a partial spectrum width $\tilde{\sigma}^2_{\mathrm{V}}$, which is the spectrum width for the small average subregion of a resolution volume occupied by each SC. The complete spectrum width over a resolution volume σ^2_{V} can be expressed as a sum of several contributing factors, i.e.,

$$\sigma^2_{\mathrm{V}} = \sigma^2_s + \sigma^2_\alpha + \sigma^2_d + \sigma^2_o + \sigma^2_t \tag{9}$$

where σ^2_s is due to shear, σ^2_α is a result of antenna motion, σ^2_d arises from varying speeds of fall for different hydrometeors, σ^2_o is due to hydrometeor oscillation, and σ^2_t is the contribution of turbulence [46]. σ^2_α is not relevant to electronically scanning arrays, σ^2_o does not apply here as our simulator does not model drop oscillation, and σ^2_t is accounted for by the random component of the SC velocities. Therefore, $\tilde{\sigma}^2_{\mathrm{V}}$ can be expressed as [46]

$$\tilde{\sigma}^2_{\mathrm{V}} = \sigma^2_s + \sigma^2_d \tag{10}$$

$$\sigma^2_d = (\sigma_{d0} \sin\theta_e)^2 \tag{11}$$

$$\sigma^2_s = (r_0\sigma_\theta k_\theta)^2 + (r_0\sigma_\phi k_\phi)^2 + (\sigma_r k_r)^2 \tag{12}$$

where r_0 is the range from the radar to the center of the resolution volume; $\sigma_{d0} \approx 1\ \mathrm{m}\cdot\mathrm{s}^{-1}$ is the spread in hydrometeor terminal velocity [46]; θ_e is the angle of elevation of the raindrop; and k_θ, k_ϕ, and k_r are the components of wind shear in each dimension of a spherical coordinate system with the radar at the origin. Calculation of σ^2_s is complicated by the fact that, ordinarily, σ_θ and σ_ϕ are the second moments of the antenna pattern beamwidth and σ_r is the second moment of the range weighting function. Because we are trying to determine spectrum widths for some small subregion of the radiation pattern, we must estimate the second moments of the pattern over those regions. First, the average size of the subvolume occupied by each SC is calculated. This is defined as the region surrounding each SC for which it is the nearest SC to any enclosed point. Because the SCs are randomly distributed throughout the simulation volume with a uniform probability density function, it can be assumed that this mean subvolume size is uniformly valid throughout the simulation volume. Second, it is assumed that this average subvolume size is sufficiently small such that the hydrometeor properties, the antenna radiation pattern, and the range weighting function can reasonably be approximated as constant within it. Given these assumptions, σ_θ and σ_ϕ may now represent the second moment of a uniform weighting function across each dimension of the solid angle represented by each SC, and σ_r may represent the second moment of a uniform weighting function across the range region represented by each SC. These parameters, namely, Z_{H}, Z_{V}, Φ_{DP}, ρ_{HV}, and $\tilde{\sigma}^2_{\mathrm{V}}$, together with the ARPS-specified wind field (used to generate Doppler shifts), comprise all the necessary information to determine the expected parameters of a signal reflected from any point in the simulation volume.

B. SCs

A perfectly realistic weather simulator would derive a received signal based on a summation of the reflected signals from every individual hydrometeor in a simulation volume. However, due to the shear number of hydrometeors present in a weather system that spans hundreds or thousands of cubic kilometers, this is computationally intractable for large-scale simulations. In order to solve this problem, the proposed simulator simplifies the calculation by populating the simulation volume with SCs, point targets with scattering parameters that represent the properties of the entire distribution of hydrometeors within some region in the simulation space.

1) SC Motion: The scheme used to move the SCs through space is drawn directly from Cheong *et al.* [24]. This process is critical to the simulation, as it is the method through which Doppler shifts are introduced to the signals measured by the simulated radar. SCs are initialized at random positions throughout the simulation volume based on some specified sampling density. At every time step corresponding to 1 pulse repetition time (PRT), a received signal is composed through methods discussed later in this paper. Afterward, the positions of the scatters are updated based on their velocity and the PRT length. This process can be expressed as follows:

$$\mathbf{s}^{(k)}(n) = \mathbf{s}^{(k)}(n-1) + \mathbf{v}^{(k)}(n-1)T_s \tag{13}$$

where $\mathbf{s}^{(k)}(n) = [x\ y\ z]$ is the position vector of the kth SC at time step n, $\mathbf{v}^{(k)}(n) = [\tilde{u}\ \tilde{v}\ \tilde{w}]$ is the velocity vector of the kth SC at time step n, and T_s is the PRT length. Each velocity component is obtained from the wind velocities and TKEs of the ARPS grid as follows [24]:

$$\tilde{u} = u + \epsilon\sqrt{\frac{2}{3}\mathrm{TKE}} \tag{14}$$

$$\tilde{v} = v + \epsilon\sqrt{\frac{2}{3}\mathrm{TKE}} \tag{15}$$

$$\tilde{w} = w + \epsilon\sqrt{\frac{2}{3}\mathrm{TKE}} \tag{16}$$

where ϵ is the output of a normally distributed unit variance random number generator. SCs that move out of the simulation volume are replaced with new SCs initialized at random positions in the volume. One potential issue with allowing the SCs to move with the wind field is that our effective sampling density can be affected by the divergence of the wind field. If a divergent wind field were allowed to move the SCs for too long without any intervention, it would create a region with few, if any, SCs to return a signal to the simulated radar. To avoid this problem, a small proportion of the SCs are randomly replaced after each PRT.

2) Physical SC Characteristics: The amplitude and phase of the scattering parameters of each SC change in time due to two factors. The first is a pair of unit power weather-like random signals (one associated with horizontal polarization and the other with vertical) associated with each SC. The second is the set of atmospheric conditions at the location of the SC at any point in time. The weather-like signals serve a twofold purpose. First, since each SC represents a small region of weather, these signals imbue the reflected signals from the

SC with realistic statistical properties consisting of a Rayleigh distributed amplitude and uniformly distributed phase [46]. Second, they allow for the correlation coefficient of the H and V signals to be set according to the values calculated from the ARPS model. At the beginning of each simulation, the method described by Zrnic [20] is used to generate two independent random signals with the desired Doppler spectrum, designated $w_1[n]$ and $w_2[n]$. The Doppler spectra of these signals have a zero-mean Doppler velocity (since this is introduced by the motion of the SC in space), unit power, and a Doppler spectrum width $\tilde{\sigma}$ determined from the ARPS model. $w_1(n)$ serves as weather-like signal associated with horizontal polarization. As outlined by Galati and Pavan [21], $w_1[n]$ and $w_2[n]$ are then used to create a third sequence $w_3[n]$, which will have some desired correlation coefficient ρ_{HV} with $w_1[n]$. This is done according to the following equation:

$$w_3[n] = \rho_{\mathrm{HV}} w_1[n] + \sqrt{1 - |\rho_{\mathrm{HV}}|^2} w_2[n]. \tag{17}$$

$w_3[n]$ becomes the weather-like signal associated with vertical polarization. The appropriate values of $Z_{\mathrm{H}}(\vec{r})$, $Z_{\mathrm{V}}(\vec{r})$, and $\phi_{\mathrm{DP}}(\vec{r})$ for the SC at each time step are found through quad linear interpolation from the ARPS model as described by Cheong *et al.* [24] Once these values have been obtained, they are combined with each SC's associated weather-like signals to form its final scattering parameters for the current time step, i.e.,

$$S_{\mathrm{HH}}(\vec{r}, n) = \alpha \sqrt{Z_{\mathrm{H}}(\vec{r})} w_1[n] \tag{18}$$

$$S_{\mathrm{VV}}(\vec{r}, n) = \alpha \sqrt{Z_{\mathrm{V}}(\vec{r})} w_3[n] \exp\left(j\phi_{\mathrm{DP}}(\vec{r})\right) \tag{19}$$

where α is a scaling factor introduced to decouple the user-configurable SC density from the total returned power, such that the expected reflectivity values at each range gate remain constant regardless of the configured SC density.

III. Radar System Model

The primary objective of this simulator is to model the effects of PPAR design decisions on weather observations. As such, the level of detail and flexibility offered by the simulated system model is critical. The simulator incorporates the basic system parameters of center wavelength λ, pulsewidth τ, and PRT. In order to simulate arrays, it allows for customizable element radiation patterns, positions, and amplitude weights, as well as adjustable transmit polarization. For added realism, it also provides an option to incorporate adjustable random phase and amplitude errors into the array pattern calculation. The mechanical position of the array and the beam positions for each scan are also fully configurable. In order to allow for experimentation with advanced beamforming techniques on receive, the simulator provides an option to generate separate time series data for each array element. Transmitted waveforms are also fully configurable, with their effects modeled through conversion to a range weighting function that accounts for quantization effects. Similarly, the waveform characteristics from pulse to pulse, such as transmit phase and relative amplitude of the H and V pulses, are entirely customizable.

A. Antenna

Full description of the radiation from a dual-polarization array requires eight different patterns. The patterns $F_{\mathrm{HH}}(\theta, \phi, \theta_s, \phi_s)$ and $F_{\mathrm{VV}}(\theta, \phi, \theta_s, \phi_s)$, where θ is elevation and ϕ is azimuth with respect to array broadside and θ_s and ϕ_s specify the current scan angle, specify the copolar radiation patterns in the horizontal and vertical planes, respectively. In other words, they describe the H-polarized radiation induced by an excitation of the H port of the antenna and the V polarized radiation induced by an excitation of the V port. The cross-polar pattern $F_{\mathrm{HV}}(\theta, \phi, \theta_s, \phi_s)$ specifies the H radiation induced by a V port excitation, and $F_{\mathrm{VH}}(\theta, \phi, \theta_s, \phi_s)$ specifies the V radiation induced by an H port excitation. For many systems, including the one simulated herein, the transmit and receive patterns differ due to different complex weights placed on each element on transmit and receive. In this case, which is assumed in ensuing equations, a superscript of Tx or Rx is added to the variable names earlier to distinguish transmit and receive patterns, respectively. For a phased array, each of these patterns is the product of a polar element pattern describing the field radiated from an individual element in the array and an array factor calculated based on the spatial positions of the elements and their complex weights. The polar element patterns (see Fig. 1) are direct inputs to the simulator. They consist of a set of four complex-valued patterns, each of which is an azimuth/elevation table of the radiated field from -90° to 90° from broadside in each direction. The array factor is calculated within the simulator through simple beamforming using the desired complex weights and specified random errors. In order to model electronic steering, a separate array factor must be calculated for every beam position in the simulated scan for both transmit and receive. An example set of complete radiation transmit patterns is shown in Fig. 2. These patterns are incorporated into the radar range equation model used in our simulator using the method developed in [47, Section 5.3]. This model can be expressed as follows:

$$\begin{aligned}\begin{bmatrix} V'_{\mathrm{H}} \\ V'_{\mathrm{V}} \end{bmatrix} &= \begin{bmatrix} F_{\mathrm{HH}}(\theta, \phi, \theta_s, \phi_s)^{\mathrm{Rx}} & F_{\mathrm{VH}}(\theta, \phi, \theta_s, \phi_s)^{\mathrm{Rx}} \\ F_{\mathrm{HV}}(\theta, \phi, \theta_s, \phi_s)^{\mathrm{Rx}} & F_{\mathrm{VV}}(\theta, \phi, \theta_s, \phi_s)^{\mathrm{Rx}} \end{bmatrix} \\ &\quad \times \begin{bmatrix} S_{\mathrm{HH}}(\vec{r}, n) & 0 \\ 0 & S_{\mathrm{VV}}(\vec{r}, n) \end{bmatrix} \\ &\quad \times \begin{bmatrix} F_{\mathrm{HH}}(\theta, \phi, \theta_s, \phi_s)^{\mathrm{Tx}} & F_{\mathrm{HV}}(\theta, \phi, \theta_s, \phi_s)^{\mathrm{Tx}} \\ F_{\mathrm{VH}}(\theta, \phi, \theta_s, \phi_s)^{\mathrm{Tx}} & F_{\mathrm{VV}}(\theta, \phi, \theta_s, \phi_s)^{\mathrm{Tx}} \end{bmatrix} \begin{bmatrix} X_{\mathrm{H}} \\ X_{\mathrm{V}} \end{bmatrix}.\end{aligned} \tag{20}$$

where the values V'_{H} and V'_{V} represent received voltages normalized for the effects of target range and range weighting function.

The model can be also expressed more succinctly as

$$\mathbf{V}' = \mathbf{F_{Rx} S F_{Tx} X} \tag{21}$$

where X_{H} and X_{V} are the complex-valued H and V port excitations on the array, respectively; and $S_{\mathrm{HH}}(\vec{r}, n)$ and $S_{\mathrm{VV}}(\vec{r}, n)$ are the copolar scattering parameters calculated for that scatterer and at its current position $\vec{r}$ and simulation time step n. The terms of the scattering matrix not on the main diagonal are the cross-polar scattering coefficients, which are equal to 0 due to the assumption of a zero-mean canting angle distribution

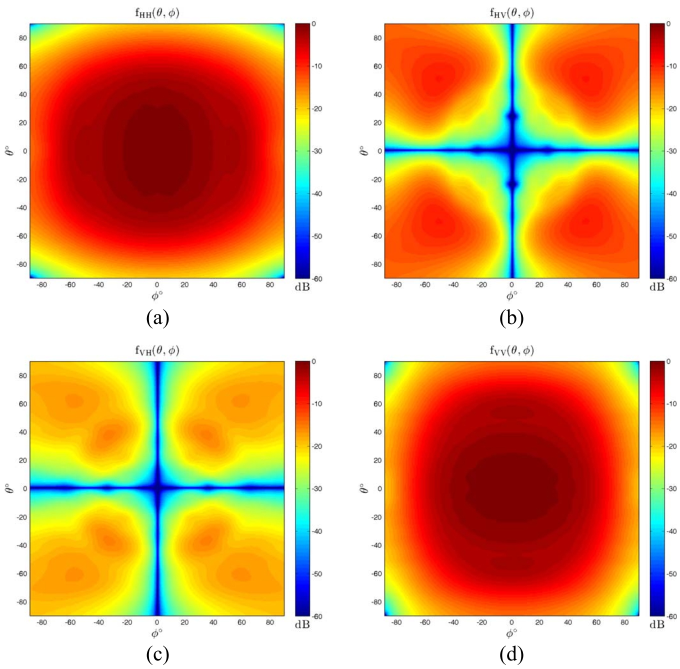

Fig. 1. Copolar and cross-polar electric fields of the patch antenna model used to obtain the simulation results. θ is elevation and ϕ is azimuthal angle with respect to the broadside angle of the element. Polarization measurements are in Ludwig II. These are High Frequency Structural Simulator (HFSS) simulations of the element patterns of the Lincoln Labs Generation II panels currently in service on the Ten Panel Demonstrator, a polarimetric planar array currently under evaluation by the National Severe Storms Laboratory. (a) Copolar radiation pattern of H-polarized patch. (b) Cross-polar radiation pattern of H-polarized patch. (c) Cross-polar radiation pattern of V-polarized patch. (d) Copolar radiation pattern of V-polarized patch.

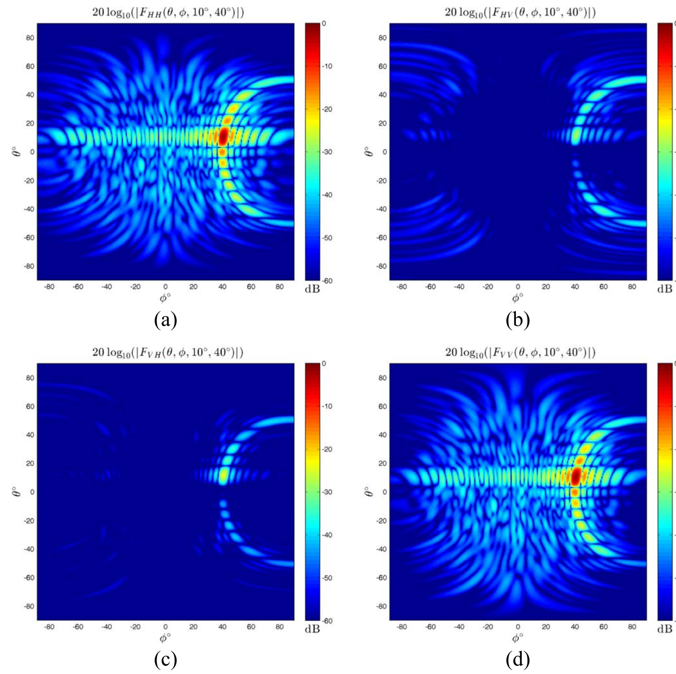

Fig. 2. Radiation power patterns on transmit for the simulated array. θ is elevation and ϕ is azimuthal angle with respect to the broadside angle of the array. Polarization measurements are in Ludwig II. Each pattern is the product of the corresponding element pattern with an array factor that includes random phase and amplitude errors, which are responsible for the evident spurious sidelobes. The array patterns shown here are electronically steered to $\theta = 10°$, $\phi = 40°$. The array geometry and elements weights used are identical to those of the Ten Panel Demonstrator. (a) Copolar radiation pattern of H-polarized array. (b) Cross-polar radiation pattern of H-polarized array. (c) Cross-polar radiation pattern of V-polarized array. (d) Copolar radiation pattern of V-polarized array.

with small variance among the hydrometeors represented by each SC [31]. It should be noted that our definition of the scattering matrix $\mathbf{S}$ differs from its standard usage in two key ways. One is that, here, it represents a scattering parameter for an ensemble of particles rather than an individual hydrometeor. This reduction of an ensemble of particles to an equivalent point target that has scattering parameters with weather-like properties is a well-established practice in time series weather radar simulators (see [22], [27], and [28]). The other distinction is that $S_{\mathrm{VV}}(\vec{r}, n)$ incorporates the differential propagation phase. In reality, this effect occurs gradually along the transmitted pulse's propagation path, but as a measure to reduce computational complexity, we precalculate this value from ARPS data and apply it at the pulse's point of contact with the SC. The radiation patterns for the current steering angle exist as a set of lookup tables in azimuth and elevation. For each SC, the value of each pattern at its precise angle relative to the radar is calculated by a bilinear interpolation on the corresponding table.

An additional consideration taken into account by the simulator is the effect of mechanical tilt on both steering angles and polarization. Consider a Cartesian coordinate system xyz, which will be referred to as the absolute coordinates. There is a planar array in the $y-z$ plane with its broadside oriented along the positive x-axis, where the $x-y$ plane is parallel to Earth's surface. Next, consider rotating this array about the y-axis by some angle θ_e. Now, the array's broadside direction can be used to define a new coordinate system $x'y'z'$, where x' is the new broadside direction. These coordinates will be referred to as the array-relative coordinates and can be calculated as

$$x' = x \cos\theta_e + z \sin\theta_e \tag{22}$$

$$y' = y \tag{23}$$

$$z' = -\,x \sin\theta_e + z \cos\theta_e. \tag{24}$$

From these two sets of coordinates, the absolute azimuth ϕ and inclination θ and the relative azimuth θ' and ϕ' can be calculated through the standard procedure for conversion to spherical coordinates. The radiation patterns of the array are necessarily given in terms of array-relative coordinates, with Ludwig II polarization directions corresponding to the unit vectors $\hat{\phi}'$, $\hat{\theta}'$. However, the scatterer positions are in absolute coordinates; furthermore, the local horizontal and vertical polarization directions at the SCs are defined by the unit vectors $\hat{\phi}$ and $\hat{\theta}$, respectively. The effects of this transformation are illustrated in Fig. 3 and are thoroughly examined by Orzel in [48, Ch. 5] for the case of an array with 1-D beam steering. The only difference between his work and the results presented here is that the array-relative beam inclination θ' is allowed as a free variable. The transformation creates two major consequences within the simulator. The first is that the absolute angles θ, ϕ must be converted to θ', ϕ' both when calculating the necessary electronic steering angles in order to scan some region of space and when using the calculated radiation patterns to determine

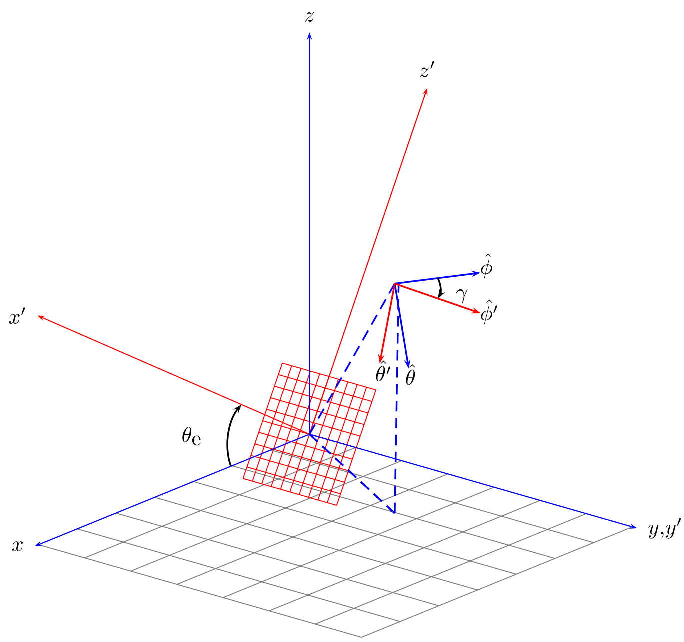

Fig. 3. This diagram shows the spatial relationship between the absolute coordinate system (xyz) and the array relative coordinate system ($x'y'z'$). It also shows the angle γ between the basis of the radiated polarization as measured in Ludwig II ($\hat{\phi}, \hat{\theta}$) and the local H and V polarization directions at a hydrometeor ($\hat{\phi}$ and $\hat{\theta}$, respectively). The red grid represents the array face.

the energy reflected by each SC in the volume. This is accomplished through the following set of equations:

$$\theta' = \arccos\left(\cos\theta\cos\theta_e - \sin\theta\cos\phi\sin\theta_e\right) \tag{25}$$

$$\phi' = \arctan\left(\frac{\sin\theta\sin\phi}{\sin\theta\cos\phi\cos\theta_e + \cos\theta\sin\theta_e}\right). \tag{26}$$

The second consequence is that the horizontal and vertical polarization directions $\hat{\theta}'$, $\hat{\phi}'$ are rotated by some angle γ with respect to the local polarization directions at the SCs if the beam is electronically steered in the array-relative azimuth direction. γ may be calculated as follows:

$$\gamma = \arccos\left(\cos\theta_e\sin\phi\sin\phi' + \cos\phi\cos\phi'\right). \tag{27}$$

This effect is accounted for by projecting the array-relative polarization components onto the absolute polarization basis on transmit and projecting it back to array-relative on receive. This is accomplished by inserting the appropriate rotation matrices into (21), yielding

$$\mathbf{V}' = \mathbf{F_{Rx}}\mathbf{P^T}\mathbf{s}'\mathbf{P}\mathbf{F_{Tx}}\mathbf{X} \tag{28}$$

where

$$\mathbf{P}(\gamma) = \begin{bmatrix}\cos\gamma & \sin\gamma\\ -\sin\gamma & \cos\gamma\end{bmatrix} \tag{29}$$

$$\mathbf{P}(-\gamma) = \mathbf{P}^{-1}(\gamma) = \mathbf{P}^T(\gamma). \tag{30}$$

B. Waveform Design

The simulator accepts a waveform design as some function of baseband frequency over time. It then converts this function to an actual baseband waveform. In doing so, it emulates the operation of an actual direct digital synthesizer by quantizing the waveform to a specified number of possible phase and amplitude states. A range weighting function $W(r)$ is then derived from the waveform by taking its autocorrelation function. For each SC in a resolution volume, a range weight is approximated from the calculated function through linear interpolation.

There are four modes of polarimetric signal transmission implemented in the simulator. They include the two most common modes of signal transmission in polarimetric radars, namely, simultaneous horizontal and vertical (SHV) and alternating horizontal and vertical (AHV). They also include two recently proposed methods of signal transmission, namely, pulse-to-pulse PCSHV and QSHV. These were proposed specifically in order to reduce the effects of cross-coupling bias while retaining many of the advantages associated with SHV [31].

PCSHV (see [9] and [10]) operates by modulating the excitation voltage on either the H or the V port with some phase code $c[n]$, where n is the index of the particular pulse within the coherent processing interval. $c[n]$ is chosen such that the Doppler spectrum of the first-order cross-polar contamination (from the H channel returns produced by the V channel transmission, and vice versa) is shifted by one half the Nyquist interval relative to the copolar signal. The code currently used by the simulator is [10]

$$c[n] = \exp(j\pi n). \tag{31}$$

Upon reception, the signal in the receive channel is first decoded. In the particular case of this code, this can be accomplished by simply multiplying the received signal by the original code. Then, it is processed as in SHV mode. The first-order contamination will cancel itself during coherent integration of each processing interval, assuming an even number of pulses [10].

The second proposed method of signal transmission, i.e., QSHV, operates by transmitting the H and V pulses separately, but in immediate succession on each PRT [10]. This has the effect that, at any given time, the signal being received by the radar in H corresponds to a different range gate than that being received in V. The resulting decorrelation between the copolar signal and the cross-polar contamination results in a reduction in observed bias. The only special processing necessary on receive is to correct the range shift such that the H and V range gates align. The signal may then be processed as in SHV [10].

C. Coherent Integration

At each time step, the simulator composes a time series point for every radar resolution volume in the scan. For each resolution volume, the signal is composed as a coherent integration of signals returned from every SC within the range annulus defined by the resolution volume's range and the pulsewidth. This signal can be expressed as

$$V_{\mathrm{H}} = \sum_{k=0}^{N'-1}\frac{W\left(r^{(k)} - r_0\right)}{r^{(k)2}}V_{\mathrm{H}}'^{(k)}\exp\left(j\frac{4\pi r^{(k)}}{\lambda}\right) + \mathcal{N}_{\mathrm{H}} \tag{32}$$

$$V_{\mathrm{V}} = \sum_{k=0}^{N'-1}\frac{W\left(r^{(k)} - r_0\right)}{r^{(k)2}}V_{\mathrm{V}}'^{(k)}\exp\left(j\frac{4\pi r^{(k)}}{\lambda}\right) + \mathcal{N}_{\mathrm{V}} \tag{33}$$

where N' is the number of SCs present in the range annulus,

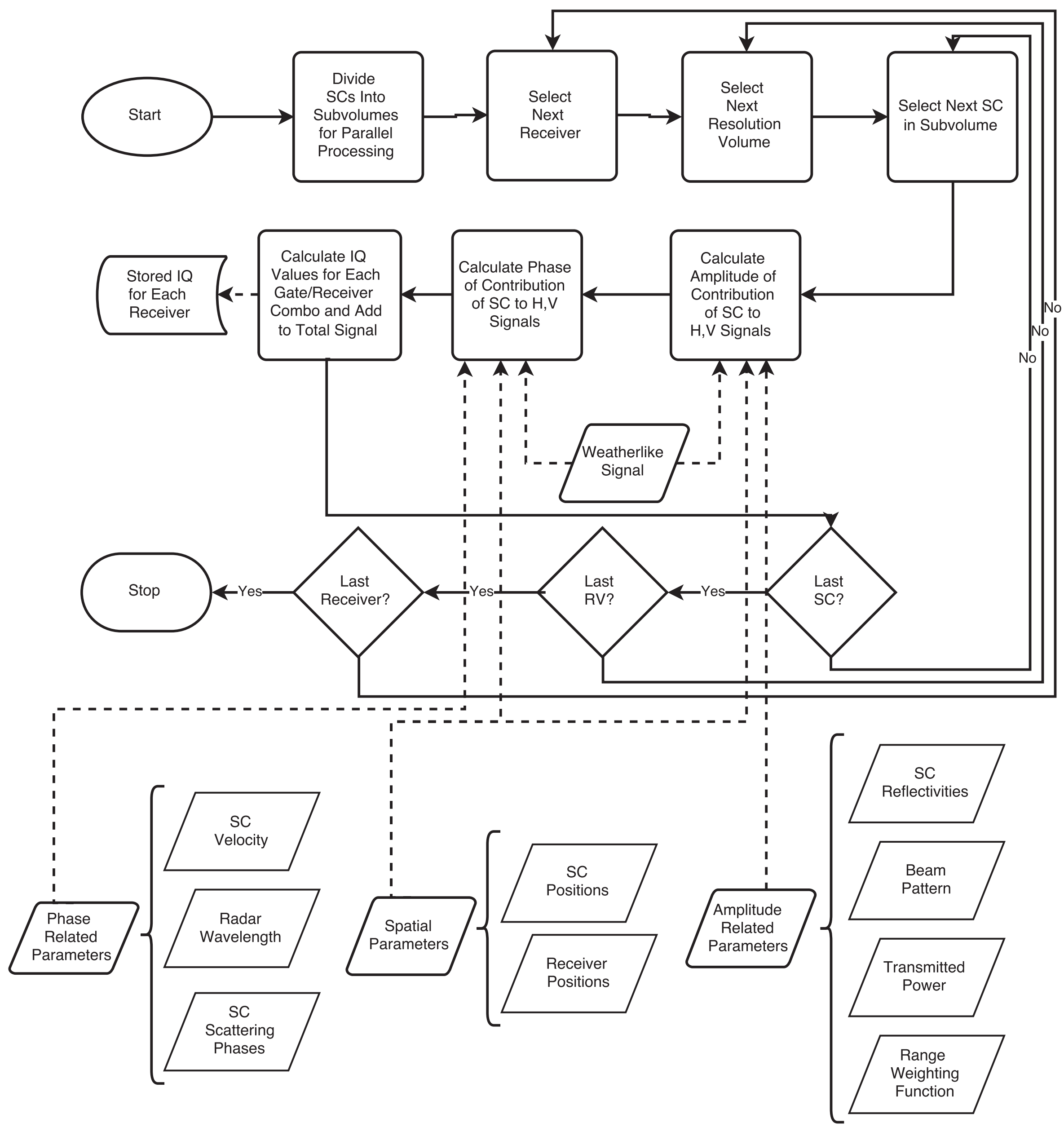

Fig. 4. Diagram of the coherent integration process. "Scattering center" is abbreviated here as SC. The upper portion of the diagram outlines the actual process, whereas the parallelograms below give a breakdown of the various inputs to the algorithm.

$W(r)$ is the range weighting function, r_0 is the range to the center of the range annulus, $r^{(k)}$ is the range of the kth SC, V'_{H} and V'_{V} are the values of the polarimetric scattering/radiation model given by (20), and $\mathcal{N}_{\mathrm{H}}$ and $\mathcal{N}_{\mathrm{V}}$ are simulated thermal noise added to each channel. This process is illustrated in Fig. 4.

Some example PPAR observations were simulated under a variety of conditions in order to illustrate effects on data quality due to changes in system configuration and atmospheric conditions. These simulations are all scans of the same volume of simulated weather with the same position relative to the array's location (centered at 3° in elevation and 0° in azimuth relative to the array). This simulated weather scenario is depicted by the single-elevation slices of ARPS-derived radar measurables shown in Fig. 6. The parameters varied between the simulations included the mechanical elevation tilt of the array (θ_e), the differential phase assumed to have accumulated as the transmitted pulse propagated between the array and the simulated weather volume (ϕ_{DP0}), and the transmit mode of the radar. Fig. 5(a) shows the result of an SHV scan with $\theta_e = 3°$ and $\phi_{\mathrm{DP0}} = 122°$. Because of the small mechanical elevation and electronic scan angles, the observed values of all three polarimetric products correlate very strongly with the ground truth values shown in Fig. 6. Fig. 5(b) shows a scan in SHV with ϕ_{DP0} held constant, but θ_e increased to 10°. Because of the increased mechanical tilt and electronic scan angles, the quality of the Z_{DR} data obtained is significantly degraded, more so at angles farther away from array broadside. Fig. 5(c) shows the results of performing a scan under identical conditions, but in PCSHV mode. Using the PCSHV transmit mode, the quality of the Z_{DR} data is significantly improved at the expense of some accuracy in estimates of ρ_{HV}. The final simulation, shown in Fig. 5(d), illustrates the dependence of these biases

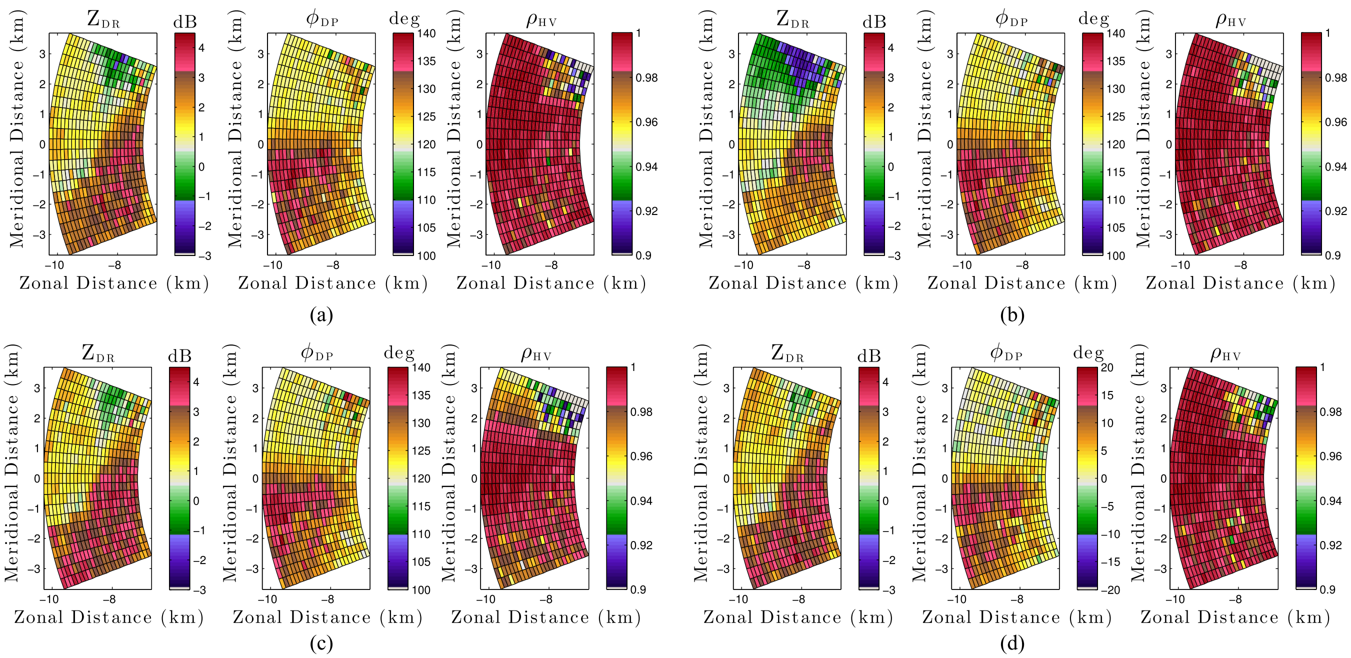

Fig. 5. Representative simulator output obtained under several different sets of simulator conditions. The PPIs are all of the same scan volume, centered at an elevation of 3° with respect to the radar. Parameters varied include the mechanical elevation tilt of the array (θ_e), the initial differential phase at the point in the simulation volume nearest the array (ϕ_{DP0}), and transmit mode (SHV or PCHV). (a) SHV, $\theta_e = 3°$, $\phi_{\mathrm{DP0}} = 122°$. (b) SHV, $\theta_e = 10°$, $\phi_{\mathrm{DP0}} = 122°$. (c) PCSHV, $\theta_e = 10°$, $\phi_{\mathrm{DP0}} = 122°$. (d) SHV, $\theta_e = 10°$, $\phi_{\mathrm{DP0}} = 0°$.

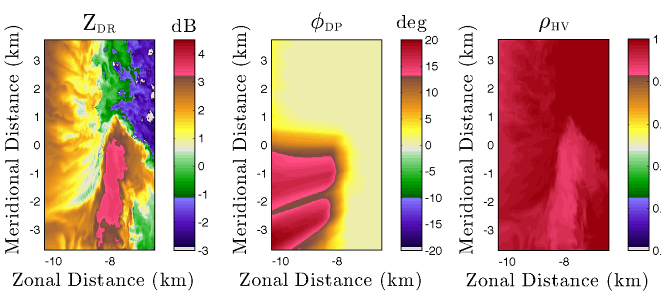

Fig. 6. ARPS data consisting of a single elevation cross section intersecting the volume scanned by the radar in each of the example simulations performed.

on differential phase. This scan was taken at $\theta_e = 10°$ in SHV mode, but with $\phi_{\mathrm{DP0}} = 0°$. This lower differential phase value reduces the observed biases to low levels comparable with what is observed at $\theta_e = 3°$.

The simulated radar configuration that produced these results uses a modification of the polarimetric element patterns shown in Fig. 1 to simulate perfect copolar calibration (i.e., the H copolar pattern was also used as the copolar pattern for V). The element and array patterns are the result of HFSS simulations based on an antenna design presented by Conway *et al.* [49]. The planar array geometry was a 2 × 5 array of panels, each of which consists of an 8 × 8 array of radiating elements. The simulated radar operated at S-band, transmitting 40-μs pulses (with a range resolution of 125 m due to pulse compression) with a 1-ms PRT and a 30-pulse coherent processing interval. The thermal noise added to the signal was designed to yield a mean SNR of 60 dB across the field of observed resolution volumes. One additional key simulation parameter is the phase difference between the excitations X_{H} and X_{V} on the array elements. This affects both bias magnitude and the particular values of differential phase that will introduce the most bias to radar observations. This simulator configuration is summarized in Table I.

TABLE I
SIMULATOR CONFIGURATION

Element Configuration	16 x 80
Beamwidth	7° x 3°
Element Spacing	0.48 λ
SD of Phase Error	5°
SD of Amplitude Error	0.5 dB
Operating Frequency	2.85 GHz
Pulse Repetition Time	1 ms
Pulse Width	40 μs
Frequency Modulation	Linear
Bandwidth	2.7 MHz
Pulse Window	Blackman
3dB Range Resolution	125 m
Peak Range Sidelobe Level	-85.4 dB
Mean SNR	60 dB
$\angle X_{\mathrm{H}} - \angle X_{\mathrm{V}}$	208°

IV. CONCLUSION

The simulator presented here combines the Lagrangian SC framework demonstrated by Cheong *et al.* [24] with realistic antenna patterns, as well as the method of time series generation developed by Zrnic [20] and extended by Galati and Pavan [21] method of time series generation in order to produce time series which account for the existence of cross-polar fields. The ARPS is used to characterize the effects of cross-polar fields on the observation of realistic weather scenarios. In order to enable accurate studies of these effects across a wide variety of possible system configurations, a detailed and flexible model of a PPAR system has been implemented. It includes easily configurable polar element patterns, array geometry, and waveform design, as well as simultaneous (SHV), alternating (AHV), PCSHV, and QSHV transmit schemes. This combination of the most current techniques for weather simulation with this level of detail and flexibility in modeling radar systems allows for realistic emulation of the challenges and mitigation techniques that have been theorized for PPAR weather observation.

There are many possibilities for future studies using this simulation framework. One of the most obvious is a thorough evaluation and comparison of polarimetric product biases using each of the available transmission schemes. Another possibility is that it could be used to simulate and evaluate array calibration procedures. The flexibility of the radar model could also be used to test additional methods of cross-polar contamination mitigation such as cylindrical array geometries. The ability to generate time series data for individual elements could be used to explore the possibilities of advanced beamforming with PPARs. Additionally, the simulator may be used to develop a system for benchmarking PPAR data quality through comparisons with a colocated parabolic dish with a much smaller beamwidth. Such a procedure would promise to be extremely useful in evaluating the performance of the first experimental PPARs.

There are also a number of potential improvements to the simulator that could be made in the course of future work. One limitation of the current framework is the fact that the simulator models transmitted signals as single complex values in order to generate time series signals more directly. Waveform design is accounted for in the simulator through precalculation of a range weighting function that is applied to the scatterers within each resolution volume. While the current approach offers major reductions in computational demand, it also severely limits the ability of the simulator to model system configurations that feature waveform diversity, such as multiple-input–and multiple-output techniques [50], or the use of waveform design to gain isolation between array faces [51] or polarizations [52]. Consequently, significant architectural changes would be needed to accurately simulate waveform diversity. One possible implementation, which would retain the current system of modeling transmitted signals as single values, would be to run a separate simulation for each transmitted waveform. Every waveform would have its own range weighting function, and the cross-correlation between each given waveform and all other waveforms would be precalculated and used during simulation to accurately model the crosstalk between transmitted signals. An alternative would be to change the simulation architecture, such that the transmitted signal is modeled not as a single complex value, but as a densely sampled baseband waveform. Each transmitted waveform would be phase shifted and attenuated through the simulator's model of transmission, backscattering, and reception, much like the complex excitation values X_{H} and X_{V} in the current architecture. However, each received waveform would also need to be appropriately time delayed based on two-way propagation time to compose the received signal (an operation corresponding to the division of the scatterers into range gates when simulating using a single-value transmitted signal). The results of this operation for all waveforms would be summed to form a single composite signal. A matched filtering operation would then be performed for each waveform to produce separate streams of time series values. This operation would eliminate the need to precalculate range weighting functions for each waveform and cross correlations for each waveform pair.

Additionally, there are a pair of limitations related to the forward operator used to derive radar observable parameters from the ARPS model data. The first is the use of fixed closed-form expressions to determine the scattering characteristics of hydrometeors. The equations from [40] used to calculate Z_{H}, Z_{V}, and K_{DP} contain constants derived from T-matrix calculations at S-band. Therefore, the simulator will not accurately reflect non-Rayleigh scattering effects that would occur at shorter operating wavelengths. The same limitation exists for the Rayleigh–Gans assumption used to calculate ρ_{HV}. In order to accurately study polarimetric signatures of rain at shorter wavelengths, or of very large hydrometeors at S-band, the simulator could be modified to allow for radar observable calculations based on user-provided scattering parameter data. The second forward operator limitation is the highly constrained DSD model. In order to improve the accuracy of the polarimetric signatures derived from the model data, the fixed-intercept single-moment variant of the constrained gamma DSD currently in use could be replaced with the more flexible and more widely utilized two-moment form [41]. While the current version of the simulator is very useful for characterizing the effects of system design on the accurate measurement of Z_{DR}, Φ_{DP}, and ρ_{HV}, improvements to the forward operator should be strongly considered before utilizing the simulator to estimate the effects of system design on the accuracy of microphysical information retrieval (such as the performance of QPE, HCAs, or DSD retrieval algorithms). Any study of HCA performance using this simulator would also, of course, mandate an expansion of the weather model to include a variety of hydrometeor types other than rain. Finally, it would undoubtedly be of interest to implement an attenuation model, both to obtain more realistic performance data and to allow for the study of attenuation correction through the use of polarimetric products obtained by PPARs.

ACKNOWLEDGMENT

The authors would like to thank Dr. C. Fulton for numerous discussions regarding the dual-polarization antennas and J. Skala of Georgia Technology Research Institute for providing the HFSS simulations used in this work.

REFERENCES

[1] W. F. Krajewski, R. Raghavan, and V. Chandrasekar, "Physically based simulation of radar rainfall data using a space–time rainfall model," *J. Appl. Meteorol.*, vol. 32, no. 2, pp. 268–283, Feb. 1993.

[2] D. Giuli, L. Facheris, and A. Freni, "Integrated model for simulation of dual linear polarisation radar measurement fields," *Proc. Inst. Elect. Eng. F—Radar Signal Process.*, vol. 140, no. 4, pp. 223–232, Aug. 1993.

[3] E. N. Anagnostou and W. F. Krajewski, "Simulation of radar reflectivity fields: Algorithm formulation and evaluation," *Water Resour. Res.*, vol. 33, no. 6, pp. 1419–1428, Jun. 1997.

[4] G. Haase and S. Crewell, "Simulation of radar reflectivities using a mesoscale weather forecast model," *Water Resour. Res.*, vol. 36, no. 8, pp. 2221–2231, Aug. 2000.

[5] O. Caumont *et al.*, "A radar simulator for high-resolution nonhydrostatic models," *J. Atmos. Ocean. Technol.*, vol. 23, no. 8, pp. 1049–1067, Aug. 2006.

[6] R. M. May, M. I. Biggerstaff, and M. Xue, "A Doppler radar emulator with an application to the detectability of tornadic signatures," *J. Atmos. Ocean. Technol.*, vol. 24, no. 12, pp. 1973–1996, Dec. 2007.

[7] A. Lupidi *et al.*, "Polarimetry applied to avionic weather radar: Improvement on meteorological phenomena detection and classification," in *Proc. TIWD/ESAV Digit. Commun.—Enhanced Surveillance Aircraft Veh.*, Capri, Italy, 2011, pp. 73–77.

[8] C. Augros, O. Caumont, V. Ducrocq, and P. Tabary, "Development and validation of a full polarimetric radar simulator," in *Proc. 36th Conf. Radar Meteorol.*, Breckenridge, CO, USA, 2013, pp. P387-1–P387-15.

[9] V. Chandrasekar and N. Bharadwaj, "Orthogonal channel coding for simultaneous co-and cross-polarization measurements," *J. Atmos. Ocean. Technol.*, vol. 26, no. 1, pp. 45–56, Jan. 2009.

[10] D. Zrnić, R. Doviak, V. Melnikov, and I. Ivić, "Signal design to suppress coupling in the polarimetric phased array radar," *J. Atmos. Ocean. Technol.*, vol. 31, no. 5, pp. 1063–1077, May 2014.

[11] I. R. Ivic and R. J. Doviak, "Evaluation of phase coding to mitigate differential reflectivity bias in polarimetric PAR," *IEEE Trans. Geosci. Remote Sens.*, vol. 54, no. 1, pp. 431–451, Jan. 2016.

[12] I. R. Ivić, "Statistical evaluation of time multiplexing to mitigate differential reflectivity bias due to cross-polar coupling," *J. Atmos. Ocean. Technol.*, vol. 33, no. 1, pp. 127–147, Jan. 2016.

[13] D. A. Holdsworth and I. M. Reid, "A simple model of atmospheric radar backscatter: Description and application to the full correlation analysis of spaced antenna data," *Radio Sci.*, vol. 30, no. 4, pp. 1263–1280, Jul./Aug. 1995.

[14] V. Venkatesh and S. Frasier, "Simulation of spaced antenna wind retrieval performance on an X-band active phased array weather radar," *J. Atmos. Ocean. Technol.*, vol. 30, no. 7, pp. 1447–1459, Jul. 2013.

[15] A. Muschinski *et al.*, "First synthesis of wind-profiler signals on the basis of large-eddy simulation data," *Radio Sci.*, vol. 34, no. 6, pp. 1437–1459, Nov./Dec. 1999.

[16] V. Chandrasekar and V. Bringi, "Simulation of radar reflectivity and surface measurements of rainfall," *J. Atmos. Ocean. Technol.*, vol. 4, no. 3, pp. 464–478, Sep. 1987.

[17] C. Capsoni and M. D'Amico, "A physically based radar simulator," *J. Atmos. Ocean. Technol.*, vol. 15, no. 2, pp. 593–598, Apr. 1998.

[18] C. Capsoni, M. D'Amico, and R. Nebuloni, "A multiparameter polarimetric radar simulator," *J. Atmos. Ocean. Technol.*, vol. 18, no. 11, pp. 1799–1809, Nov. 2001.

[19] Z. Li, Y. Zhang, G. Zhang, and K. Brewster, "A microphysics-based simulator for advanced airborne weather radar development," *IEEE Trans. Geosci. Remote Sens.*, vol. 49, no. 4, pp. 1356–1373, Apr. 2011.

[20] D. S. Zrnic, "Simulation of weatherlike Doppler spectra and signals," *J. Appl. Meteorol.*, vol. 14, no. 4, pp. 619–620, Jun. 1975.

[21] G. Galati and G. Pavan, "Computer simulation of weather radar signals," *Simul. Pract. Theory*, vol. 3, no. 1, pp. 17–44, Jul. 1995.

[22] S. M. Torres, "Estimation of Doppler and polarimetric variables for weather radars," Ph.D. dissertation, School Elect. Comput. Eng., Univ. Oklahoma, Norman, OK, USA, 2001.

[23] B. L. Cheong, M. W. Hoffman, and R. D. Palmer, "Efficient atmospheric simulation for high-resolution radar imaging applications," *J. Atmos. Ocean. Technol.*, vol. 21, no. 2, pp. 374–378, Feb. 2004.

[24] B. Cheong, R. Palmer, and M. Xue, "A time series weather radar simulator based on high-resolution atmospheric models," *J. Atmos. Ocean. Technol.*, vol. 25, no. 2, pp. 230–243, Feb. 2008.

[25] M. Xue, K. K. Droegemeier, and V. Wong, "The Advanced Regional Prediction System (ARPS)—A multi-scale nonhydrostatic atmospheric simulation and prediction model. Part I: Model dynamics and verification," *Meteorol. Atmos. Phys.*, vol. 75, no. 3/4, pp. 161–193, Dec. 2000.

[26] M. Xue *et al.*, "The Advanced Regional Prediction System (ARPS)—A multi-scale nonhydrostatic atmospheric simulation and prediction tool. Part II: Model physics and applications," *Meteorol. Atmos. Phys.*, vol. 76, no. 3/4, pp. 143–165, Apr. 2001.

[27] R. M. May, "Estimating and mitigating errors in dual-polarization radar attenuation correction," Ph.D. dissertation, School Meteorol., Univ. Oklahoma, Norman, OK, USA, 2014.

[28] S. Lischi *et al.*, "Advanced polarimetric Doppler weather radar simulator," in *Proc. 15th IRS*, 2014, pp. 1–6.

[29] M. E. Weber *et al.*, "The next-generation multimission US surveillance radar network," *Bull. Amer. Meteorol. Soc.*, vol. 88, no. 11, pp. 1739–1751, Nov. 2007.

[30] D. Zrnic *et al.*, "Agile-beam phased array radar for weather observations," *Bull. Amer. Meteorol. Soc.*, vol. 88, no. 11, pp. 1753–1766, Nov. 2007.

[31] D. Zrnic, R. Doviak, G. Zhang, and A. Ryzhkov, "Bias in differential reflectivity due to cross coupling through the radiation patterns of polarimetric weather radars," *J. Atmos. Ocean. Technol.*, vol. 27, no. 10, pp. 1624–1637, Oct. 2010.

[32] G. Zhang, R. Doviak, D. Zrnic, and J. Crain, "Phased array radar polarimetry for weather sensing: Challenges and opportunities," in *Proc. IEEE IGARSS*, 2008, vol. 5, pp. V-449–V-452.

[33] G. Zhang *et al.*, "Phased array radar polarimetry for weather sensing: A theoretical formulation for bias corrections," *IEEE Trans. Geosci. Remote Sens.*, vol. 47, no. 11, pp. 3679–3689, Nov. 2009.

[34] D. S. Zrnic, G. Zhang, and R. J. Doviak, "Bias correction and Doppler measurement for polarimetric phased-array radar," *IEEE Trans. Geosci. Remote Sens.*, vol. 49, no. 2, pp. 843–853, Feb. 2011.

[35] L. Lei, G. Zhang, and R. J. Doviak, "Bias correction for polarimetric phased-array radar with idealized aperture and patch antenna elements," *IEEE Trans. Geosci. Remote Sens.*, vol. 51, no. 1, pp. 473–486, Jan. 2013.

[36] I. Ivić, "An approach to simulate the effects of antenna patterns on polarimetric variable estimates," presented at the 37th Conf. Radar Meteorology, Norman, OK, USA, 2015.

[37] Nov. 2009. [Online]. Available: http://www.ofcm.noaa.gov/mpar-symposium/.

[38] M. Xue, D. Wang, J. Gao, K. Brewster, and K. K. Droegemeier, "The Advanced Regional Prediction System (ARPS), storm-scale numerical weather prediction and data assimilation," *Meteorol. Atmos. Phys.*, vol. 82, no. 1, pp. 139–170, Jan. 2003.

[39] P. S. Ray *et al.*, "The morphology of several tornadic storms on 20 May 1977," *J. Atmos. Sci.*, vol. 38, no. 8, pp. 1643–1663, Aug. 1981.

[40] Y. Jung, G. Zhang, and M. Xue, "Assimilation of simulated polarimetric radar data for a convective storm using the ensemble Kalman filter. Part I: Observation operators for reflectivity and polarimetric variables," *Mon. Weather Rev.*, vol. 136, no. 6, pp. 2228–2245, Jun. 2008.

[41] C. W. Ulbrich, "Natural variations in the analytical form of the raindrop size distribution," *J. Clim. Appl. Meteorol.*, vol. 22, no. 10, pp. 1764–1775, Oct. 1983.

[42] Y.-L. Lin, R. D. Farley, and H. D. Orville, "Bulk parameterization of the snow field in a cloud model," *J. Clim. Appl. Meteorol.*, vol. 22, no. 6, pp. 1065–1092, Jun. 1983.

[43] G. Zhang, J. Vivekanandan, and E. Brandes, "A method for estimating rain rate and drop size distribution from polarimetric radar measurements," *IEEE Trans. Geosci. Remote Sens.*, vol. 39, no. 4, pp. 830–841, Apr. 2001.

[44] A. Green, "An approximation for the shapes of large raindrops," *J. Appl. Meteorol.*, vol. 14, no. 8, pp. 1578–1583, Dec. 1975.

[45] V. Bringi and V. Chandrasekar, *Polarimetric Doppler Weather Radar: Principles and Applications*. Cambridge, U.K.: Cambridge Univ. Press, 2001.

[46] R. Doviak and D. Zrnic, *Doppler Radar & Weather Observations*. Amsterdam, The Netherlands: Elsevier, 2014.

[47] C. Fulton, "Digital array radar calibration and performance monitoring techniques for direct conversion and dual polarization architectures," Ph.D. dissertation, Dept. Elect. Comput. Eng., Purdue Univ., West Lafayette, IN, USA, 2011.

[48] K. Orzel, "X-band dual polarization phased-array radar for meteorological applications, Ph.D. dissertation, Dept. Elect. Comput. Eng., Purdue Univ., West Lafayette, IN, USA, 2015.

[49] D. Conway *et al.*, "On the development of a tileable LRU for the NextGen surveillance and weather radar capability program," in *Proc. IEEE Int. Symp. Phased Array Syst. Technol.*, 2013, pp. 490–493.

[50] J. Li and P. Stoica, "MIMO radar with colocated antennas," *IEEE Signal Process. Mag.*, vol. 24, no. 5, pp. 106–114, Sep. 2007.

[51] J. M. Kurdzo, R. D. Palmer, B. L. Cheong, and M. E. Weber, "Adaptive waveform design for multi-sector array isolations," in *Proc. European Radar Conf.*, 2015, pp. 96–96.

[52] A. Pezeshki, W. Moran, S. D. Howard, and R. Calderbank, "Doppler resilient Golay complementary waveforms," *IEEE Trans. Inf. Theory*, vol. 54, no. 9, pp. 4254–4266, Sep. 2008.

Andrew D. Byrd (S'15) received the B.S. degree in electrical engineering from the Georgia Institute of Technology, Atlanta, GA, USA, in 2014. He is currently working toward the M.S. and Ph.D. degrees in electrical and computer engineering at the University of Oklahoma, Norman, OK, USA.

He is also currently a Graduate Research Assistant with the Advanced Radar Research Center, University of Oklahoma. His research interests include the design, calibration, and applications of polarimetric phased array radars.

Igor R. Ivić received the B.S. degree from the University of Novi Sad, Novi Sad, Serbia, in 1996 and the M.Sc. and Ph.D. degrees from the University of Oklahoma, Norman, OK, USA, in 2001 and 2008, respectively, all in electrical engineering.

From 1996 to 1997, he was a Research Associate with the School of Computer Science, Faculty of Technical Sciences, University of Novi Sad. In 1997, he joined the Cooperative Institute for Mesoscale Meteorological Studies, University of Oklahoma, where he was a Research Associate from 1997 to 2009 and has been a Research Scientist in the National Severe Storms Laboratory since 2009. His research interest is in weather radar signal processing, advancements of polarimetric measurements, development of algorithms for the national network of weather radars (WSR-88D), and applications of agile-beam phased array radar for weather observations.

Dr. Ivić was a recipient of the Department of Commerce Silver Medal as a member of Stormscale Research and Applications Division at the National Severe Storms Laboratory for making significant enhancements to the NEXRAD systems. He was also a recipient of the Outstanding Scientific Paper Award from the Office of Oceanic and Atmospheric Research, U.S. Department of Commerce in 2005.

Robert D. Palmer (SM'93) was born in Fort Benning, GA, USA, on June 3, 1962. He received the Ph.D. degree in electrical engineering from the University of Oklahoma (OU), Norman, OK, USA, in 1989.

From 1989 to 1991, he was a JSPS Postdoctoral Fellow with the Radio Atmospheric Science Center, Kyoto University, Kyoto, Japan, where his major accomplishment was the development of novel interferometric radar techniques for studies of atmospheric turbulent layers. After his stay in Japan, he was with the Department of Physics and Astronomy, Clemson University, Clemson, SC, USA. From 1993 to 2004, he was a part of the faculty of the Department of Electrical Engineering, University of Nebraska–Lincoln, Lincoln, NE, USA, where his interests broadened into areas including wireless communications, remote sensing, and pedagogy. Soon after moving to OU as the Tommy C. Craighead Chair in the School of Meteorology in 2004, he established the interdisciplinary Advanced Radar Research Center. He currently serves as the Executive Director of the ARRC and the Associate Vice President for Research with OU. While at OU, his research interests have focused on the application of advanced radar signal processing techniques to observations of severe weather, particularly related to phased array radars and other innovative system designs. He has published widely in the area of radar remote sensing of the atmosphere, with emphasis on generalized imaging problems, spatial filter design, and clutter mitigation using advanced array/signal processing techniques.

Prof. Palmer is a Fellow of the American Meteorological Society and has been a recipient of several awards for both his teaching and research accomplishments.

Bradley M. Isom (S'10–M'12) received the B.S. degree in computer engineering from the University of Nebraska–Lincoln, Lincoln, NE, USA, in 2005 and the M.S. and Ph.D. degrees in electrical and computer engineering from the University of Oklahoma (OU), Norman, OK, USA, in 2007 and 2012, respectively.

During his time at OU, his research interests included wind turbine clutter characterization and mitigation and advanced array and signal processing techniques. He also led the development of the Atmospheric Imaging Radar (AIR), a mobile X-band imaging radar system designed for collecting high-resolution meteorological data. He is currently a Radar Engineer with the Pacific Northwest National Laboratory (PNNL), Richland, WA, USA, where he works in support of the Atmospheric Radiation Measurement (ARM) radar instrumentation and infrastructure. At PNNL, he is responsible for developing and maintaining the ARM radar assets, as well as ensuring the delivery of quality data to end users. His current research interests include the identification and mitigation of dynamic clutter, the development of advanced signal and array processing techniques, and designing novel remote sensing platforms for atmospheric studies.

Dr. Isom is a member of the American Meteorological Society. He is also a member of Tau Beta Pi and Eta Kappa Nu honor societies.

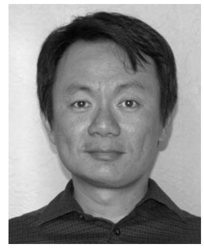

Boon Leng Cheong received the Ph.D. degree in electrical engineering from the University of Nebraska–Lincoln, Lincoln, NE, USA, in 2005, with a dissertation on adaptive beamforming to observe the atmospheric boundary layer using the turbulent eddy profiler.

He is currently a Research Scientist in the Advanced Radar Research Center and an Adjunct Assistant Professor in the School of Electrical and Computer Engineering with the University of Oklahoma, Norman, OK, USA. His research interests include software-defined radar design, array signal processing, real-time software architecture, parallel computing, and numerical radar simulation.

Alexander D. Schenkman received the B.S., M.S., and Ph.D. degrees from the University of Oklahoma, Norman, OK, USA, in 2005, 2008, and 2012, respectively, all in meteorology.

Since 2012, he has been a Postdoctoral Research Associate with the Center for Analysis and Prediction of Storms, University of Oklahoma. His major research interests center around the production and analysis of high-resolution simulations of tornadic convective systems, with a focus on the dynamics behind tornadogenesis.

Dr. Schenkman serves as an Editor for Advances in *Atmospheric Sciences* and an Associate Editor for *Monthly Weather Review*.

Ming Xue received the Ph.D. degree from Reading University, Reading, U.K.

He is currently the Weathernews Chair Professor in the School of Meteorology and the Director of the Center for Analysis and Prediction of Storms with the University of Oklahoma. He is the Principal Developer of the Advanced Regional Prediction System modeling system. His research interests include the development of advanced numerical techniques, as well as modeling and data assimilation systems; the simulation, prediction, dynamics, and predictability of mesoscale and convective-scale weather systems; tornado dynamics; and advanced assimilation and retrieval techniques for radar and other high-resolution observations.